Correcting rainfall using satellite-based surface soil moisture retrievals: The Soil Moisture Analysis Rainfall Tool (SMART)

W. T. Crow,[1] M. J. van den Berg,[2] G. J. Huffman,[3,4] and T. Pellarin[5]

Received 18 February 2011; revised 17 June 2011; accepted 6 July 2011; published 20 August 2011.

[1] Recently, Crow et al. (2009) developed an algorithm for enhancing satellite-based land rainfall products via the assimilation of remotely sensed surface soil moisture retrievals into a water balance model. As a follow-up, this paper describes the benefits of modifying their approach to incorporate more complex data assimilation and land surface modeling methodologies. Specific modifications improving rainfall estimates are assembled into the Soil Moisture Analysis Rainfall Tool (SMART), and the resulting algorithm is applied outside the contiguous United States for the first time, with an emphasis on West African sites instrumented as part of the African Monsoon Multidisciplinary Analysis experiment. Results demonstrate that the SMART algorithm is superior to the Crow et al. baseline approach and is capable of broadly improving coarse-scale rainfall accumulations measurements with low risk of degradation. Comparisons with existing multisensor, satellite-based precipitation data products suggest that the introduction of soil moisture information from the Advanced Microwave Scanning Radiometer via SMART provides as much coarse-scale (3 day, 1°) rainfall accumulation information as thermal infrared satellite observations and more information than monthly rain gauge observations in poorly instrumented regions.

Citation: Crow, W. T., M. J. van den Berg, G. J. Huffman, and T. Pellarin (2011), Correcting rainfall using satellite-based surface soil moisture retrievals: The Soil Moisture Analysis Rainfall Tool (SMART), *Water Resour. Res., 47*, W08521, doi:10.1029/2011WR010576.

1. Introduction

[2] Starting with the anticipated launch of its core satellite in 2013, land rainfall retrievals from the upcoming Global Precipitation Mission (GPM) constellation will contribute to a host of natural hazard, hydrologic, and water resource applications [*Gebremichael and Hossain*, 2009]. However, expectations for hydrologic applications are tempered by known limitations in the resolution and accuracy of satellite-based rainfall accumulation products [*Harris et al.*, 2007; *Li et al.*, 2009; *Tobin and Bennett*, 2010; *Pan et al.*, 2010]. Such products are known to suffer from a range of error sources, including sampling uncertainties [*Steiner et al.*, 2003; *Nijssen and Lettenmaier*, 2004; *Hossain et al.*, 2004], beam-filling issues [*Kummerow*, 1998], and difficulties estimating the impact of solid hydrometeors [*Bennartz and Petty*, 2001]. Over land, these difficulties are compounded by uncertainty in background emissivity values associated with variations in land surface properties [*Morland et al.*, 2001; *Bytheway and Kummerow*, 2010]. One potential strategy for ameliorating these problems is the use of ancillary land measurements related to precipitation [*Pan and Wood*, 2007; *Pellarin et al.*, 2008; *McCabe et al.*, 2008; *Pellarin et al.*, 2009]. In particular, remotely sensed surface soil moisture dynamics and rainfall share an obvious physical connection. Such synergistic opportunities are highly relevant given the likely temporal overlap between GPM and the NASA Soil Moisture Active Passive (SMAP) mission. Currently under development in anticipation of a 2014 launch, the SMAP mission will combine L band (1.4 GHz) radar and radiometry to produce a global 10 km soil moisture product with an average repeat time of 2–3 days [*Entekhabi et al.*, 2010].

[3] With this potential in mind, *Crow et al.* [2009] describe and apply a simple data assimilation approach to correct land rainfall accumulation estimates using remotely sensed surface soil moisture retrievals. Their approach is based on the time series of net additions (or subtractions) of soil water corrections calculated when sequentially assimilating surface soil moisture retrievals into a water balance model using a Kalman filter. These water volumes, or "analysis increments," are then correctively applied to the satellite-based rainfall product used to force the water balance model. Results by *Crow et al.* [2009] demonstrate that the approach can correct a substantial fraction of root-mean-square error (RMSE) in 2–10 day accumulation estimates obtained from existing multisensor, satellite-based rainfall products. That is, over land, remotely sensed surface soil moisture retrievals provide a viable source of corrective information for satellite-based rainfall products.

[1]Hydrology and Remote Sensing Laboratory, Agricultural Research Service, USDA, Beltsville, Maryland, USA.
[2]Laboratory of Hydrology and Water Management, Ghent University, Ghent, Belgium.
[3]SSAI, Greenbelt, Maryland, USA.
[4]NASA GSFC, Greenbelt, Maryland, USA.
[5]Laboratoire d'Étude des Transferts en Hydrologie et Environnement, Grenoble, France.

Copyright 2011 by the American Geophysical Union.
0043-1397/11/2011WR010576

[4] Relatively good results by *Crow et al.* [2009] are obtained despite their reliance on a simple modeling and data assimilation framework. However, such simplifications potentially contribute to specific limitations noted in their approach, particularly a tendency toward the overprediction of low-intensity rainfall events and the degradation of correlation-based rainfall accumulation skill in densely vegetated areas. In addition, the *Crow et al.* [2009] approach was validated only within the contiguous United States (CONUS) and was not directly assessed in data-poor areas, where it is likely to yield the greatest benefits.

[5] Here we will explore the potential benefit of utilizing more complex data assimilation and modeling approaches to enhance the performance of the original *Crow et al.* [2009] algorithm. On the basis of this analysis, a new approach, referred to as the Soil Moisture Analysis Rainfall Tool (SMART), is defined and tested using high-quality rain gauge data sets available within both the contiguous United States and West Africa. Finally, a quasi-global-scale analysis is conducted using rainfall data products from the Tropical Rainfall Measuring Mission (TRMM) Multisatellite Precipitation Analysis (TMPA) [*Huffman et al.*, 2007, 2010].

2. Background

[6] As noted in section 1, our baseline is the rainfall correction approach previously introduced by *Crow et al.* [2009] (hereinafter referred to as the C09 algorithm). The general algorithm development strategy employed in C09 (and continued here) is to start with simple parameterizations and add complexity only when clearly justified. Consequently, the C09 algorithm is based on using a satellite-based rainfall accumulation product (P') to derive the antecedent precipitation index (API) on day i for spatial grid box j:

$$\mathrm{API}_{i,j}^{-} = \gamma_{i,j}\,\mathrm{API}_{i-1,j}^{+} + P'_{i,j}. \tag{1}$$

In the C09 baseline, γ is estimated from the empirical relationship

$$\gamma_{i,j} = \alpha - \beta(\langle T_a \rangle_{D(i),j} - 270), \tag{2}$$

where α and $\langle T_a \rangle_{D(i)}$ is the climatological air temperature in K on the day of year D corresponding to i and α and β are global constants given in Table 1.

[7] When available, remotely sensed surface soil moisture retrievals $\theta_{i,j}$ are used to update (1) via a Kalman filter:

$$\mathrm{API}_{i,j}^{+} = \mathrm{API}_{i,j}^{-} + K_{i,j}(\theta_{i,j} - \mathrm{API}_{i,j}^{-}). \tag{3}$$

Here the minus and plus denote API values before and after Kalman filter updating, respectively. Daily soil moisture observations (in water depth dimensions) for a particular grid box are obtained by linearly rescaling a time series of raw surface soil moisture retrievals θ° (in volumetric soil moisture dimensions) such that their long-term mean (μ) and standard deviation (σ) match those derived from a multiyear integration of (1) calculated for the same grid box:

$$\theta_{i,j} = (\theta_{i,j}^{\circ} - \mu_j^{\theta})\frac{\sigma_j^{\mathrm{API}}}{\sigma_j^{\theta}} + \mu_j^{\mathrm{API}}, \tag{4}$$

where the absence of the subscript i indicates that a given variable does not vary in time.

[8] The Kalman gain K in (3) is given by

$$K_{i,j} = T_{i,j}^{-}/(T_{i,j}^{-} + S_j), \tag{5}$$

where T is the error variance for API forecasts and S is the error variance for θ retrievals. At measurement times, T is updated as

$$T_{i,j}^{+} = (1 - K_{i,j})T_{i,j}^{-}. \tag{6}$$

Between soil moisture retrievals and the adjustment of API and T via (3) and (6), API is forecasted on the basis of observed P' and (1). Likewise, T is updated via

$$T_{i,j}^{-} = \gamma_{i,j}{}^2\, T_{i-1,j}^{+} + Q_j, \tag{7}$$

where Q represents the added uncertainty in API predictions accumulated during a daily forecast step.

[9] Analysis increments are simply the change in API upon updating in (3):

$$\delta_{i,j} = \mathrm{API}_{i,j}^{+} - \mathrm{API}_{i,j}^{-} = K_{i,j}(\theta_{i,j} - \mathrm{API}_{i,j}^{-}). \tag{8}$$

If assimilated θ observations are skillful, then the corrective δ time series should correlate with recent random errors in P'. The C09 algorithm exploits this tendency to linearly correct 3 day P' sums ($[P']$) on the basis of coincident δ calculated during a soil moisture data assimilation analysis:

$$[\widetilde{P'}]_{l,j} = [P']_{l,j} + \lambda_j[\delta]_{l,j}, \tag{9}$$

where λ is a scaling factor and l now indexes nonoverlapping 3 day windows. A 3 day window appears to be the shortest accumulation window over which the C09 algorithm can be reliably applied [*Crow et al.*, 2009]. In addition, the C09 analysis was restricted to periods of liquid (i.e., nonsnow) precipitation.

[10] As discussed in C09, defining theoretical constraints for λ is difficult. Instead, C09 relies on three separate strategies: (1) calibrating time constant (but spatially variable) values of λ until the RMS error of $[\widetilde{P'}]$ is minimized relative to historical rain gauge data, (2) calibrating λ against an independent satellite-based rainfall product, or (3) simply assuming λ is a fixed constant (in both time and space). Obviously, the first approach presumes the availability of historical rain gauge data and may not be globally applicable. During calibration, any derived value of $[\widetilde{P'}] < 0$ is reset to zero.

Table 1. Assumed Values for Defined Constants Within the SMART Algorithm[a]

Constant	Equation	Value
α	(2)	0.70
β	(2)	0.01 K^{-1}
ξ	(12)	5
Q	(12)	3 mm^2

[a] Q is held externally fixed only for the case 3 methodology described in section 3.3.

[11] Because of the rescaling step in (4), the C09 procedure has no legitimate basis for correcting long-term bias in P' and can, in fact, induce a positive bias if substantial numbers of negative rainfall predictions are made and subsequently reset to zero [*Crow et al.*, 2009]. Therefore, the long-term mean of $\widetilde{P'}$ is rescaled to match that of P'. Also, to ensure that intermittent temporal data gaps in satellite-based products do not impact results, only time periods containing at least one θ° retrieval per 3 day window and one satellite-based rainfall rate estimate per day are included in the analysis. For the satellite data products considered here (see section 4), these requirements are generally met during periods of normal sensor operations.

3. Potential Modifications

[12] The C09 approach represents an intentionally simple approach to the problem of correcting rainfall accumulation amounts using soil moisture remote sensing. This section will describe a number of potential modifications incorporating increased modeling and filtering complexity. Section 5 will then evaluate modifications on the basis of their ability to improve rainfall accumulation estimates within CONUS.

3.1. Rescaling of Satellite-Based Soil Moisture Retrievals

[13] It is generally acknowledged that some type of a priori rescaling is necessary prior to the assimilation of θ° retrievals into a land surface model [see, e.g., *Reichle and Koster*, 2005; *Drusch et al.*, 2005]. In C09, such rescaling is based on the simple, time invariant transformation in (4). One shortcoming of this approach is that it fails to correct for possible seasonal differences in the climatology of modeled and remotely sensed soil moisture estimates. A second deficiency is that it corrects only for differences between the first (mean) and second (variance) statistical moments of the soil moisture time series and neglects differences in higher-order statistical moments.

[14] The first shortcoming arises because μ in (4) is a spatially variable but temporally fixed statistic sampled from a multiyear data set. To correct this, (4) can be modified so that different μ statistics are sampled separately from a multiyear data set using a 31 day sampling window centered on a particular day of the year D:

$$\theta_{i,j} = (\theta^\circ_{i,j} - \mu^\theta_{D(i),j})\frac{\sigma^{\mathrm{API}}_j}{\sigma^\theta_j} + \mu^{\mathrm{API}}_{D(i),j}. \tag{10}$$

In this way, the rescaling step in (4) is modified to vary over the seasonal cycle and compensate for possible seasonal differences existing between the API and θ° climatologies. Note that σ still does not vary seasonally in (10). A more ambitious alternative would be to introduce σ seasonality in an analogous manner.

[15] To compensate for potential differences in higher-order statistical moments, rescaling based on the cumulative density function (CDF) matching of API values to θ° can also be applied:

$$\theta_{i,j} = G_j^{-1}\left[F_j(\theta^\circ_{i,j})\right], \tag{11}$$

where F and G are the long-term CDFs of θ° and the API model, respectively. Here such transformations are based on ranking the entire historical time series of θ° and API (on a grid box by grid box basis) and transforming directly between soil moisture values in each time series with equal ranking. The nonlinear form of (11) ensures that the resulting θ time series will possess exactly the same distribution as API and not simply match its first and second statistical moments. Like (4), (11) can also be modified to capture seasonality by sampling separate F and G within a 31 day window centered on a particular D.

3.2. Conditioning of Rainfall Forecasts

[16] In order to operate effectively, the forecasting step in (1) should accurately characterize existing information concerning rainfall accumulation amounts and the impact of this information on conditioned model background uncertainty [*Crow*, 2003]. The importance of such conditioning is reflected by the considerable attention paid in recent years to developing appropriate rainfall ensembles conditioned on incomplete and inaccurate rainfall measurements and predictions [*Clark et al.*, 2004; *Hossain and Anagnostou*, 2006a, 2006b; *Wojcik et al.*, 2009]. At their most basic, such approaches recognize that no matter how uncertain, nonzero rainfall rate estimates obtained from remote sensing should lead to different conditional expectations than estimates of zero rainfall. This conditioning is not reflected in (7), where a constant additive term Q is applied at every time step, regardless of observed P'. Here, as a first step, we apply a simple approach to such conditioning by introducing a second term in (7) that induces greater amounts of background uncertainty in API forecasts when $P' > 0$:

$$T^-_{i,j} = \gamma_{i,j}{}^2\, T^+_{i-1,j} + Q_j + \xi P'^2_{i,j}. \tag{12}$$

Here the scaling factor ξ is assumed to be a unitless global constant set equal to 5 (Table 1). This change leads to larger K, and more weight applied to observations, following the observation of nonzero rainfall accumulations. If (12) provides a more appropriate background error model than (7), such temporal variations in K should lead to a more efficient integration of θ information and enhanced rainfall correction via (9). Sensitivity results describing the impact of varying ξ are described in section 5.1.

3.3. Filter Calibration

[17] The C09 approach utilizes a ν-whitening approach for constraining Q and S. In particular, it defines the time series of filtering innovations ν as

$$\nu_{i,j} = (\theta_{i,j} - \mathrm{API}^-_{i,j})/(T^-_{i,j} + S_j)^{0.5} \tag{13}$$

and adjusts the ratio Q/S until a serially white innovation time series is obtained. Such an approach is appealing because it eliminates the need to independently specify Q and S. However, recent work has shown it to be misguided because of the presence of serially correlated error in remotely sensed surface soil moisture products. In such cases, whitening ν leads to the systematical underestimation of S and excessive weight on assimilated observations in (3) [*Crow and van den Berg*, 2010].

[18] Here we instead follow the approach of *Scipal et al.* [2008] by using a triple-collocation (TC) strategy to estimate S. This approach compares soil moisture anomalies obtained from a satellite-based passive radiometer (θ'), a satellite-based scatterometer (θ'_{SCAT}), and API modeling (θ'_{API}) to obtain an estimate for the error variance in a soil moisture product:

$$S_j = \langle(\theta'_{i,j} - \theta'_{\mathrm{API},i,j})(\theta'_{i,j} - \theta'_{\mathrm{SCAT},i,j})\rangle, \tag{14}$$

where angle brackets indicate temporal averaging. Soil moisture anomalies are based on subtracting off a 31 day moving average mean obtained for each multiyear data set, and all anomalies are rescaled to have the same temporal variance as the API anomalies. Values of S obtained in this way provide an appropriate basis for estimating the spatially variable (and temporally constant) error variance of assimilated θ' observations required as input into (5) [*Crow and van den Berg*, 2010]. Q is then held globally constant at a value of 3 mm^2 (Table 1). Sensitivity results describing the impact of varying Q are described in section 5.1.

3.4. Non-Gaussian Rainfall Errors

[19] The application of a Kalman filter in the baseline C09 approach requires an implicit assumption that background modeling errors are approximately Gaussian. However, except at very coarse time and space scales, errors in rainfall observations do not generally induce Gaussian error in land surface model soil moisture predictions [*Crow*, 2003]. Consequently, better results in (9) may be obtainable using alternative filtering techniques not requiring a rigid Gaussian assumption. Both the ensemble Kalman filter (ENKF [e.g., *Reichle et al.*, 2002]) and a particle filter (PF [e.g., *Liu and Chen*, 1998]) allow this assumption to be relaxed.

[20] In an ENKF, the forecast step (1) is replaced by an N-member API ensemble generated using

$$\mathrm{API}^k_{i,j} = \gamma_{i,j}\,\mathrm{API}^k_{i-1,j} + \eta^k_{i,j}P'_{i,j}, \tag{15}$$

where η is sampled from a lognormal distribution with mean 1 and variance Λ and $k = 1, 2, \ldots, N$ is the ensemble index. Lognormal multiplicative noise of this type offers a simple way to capture conditional rainfall uncertainty and has been widely applied in ENKF land data assimilation systems [e.g., *Crow and Van Loon*, 2006; *Reichle and Koster*, 2005]. By virtue of the lognormal distribution of η, the resulting ensemble of API forecasts is non-Gaussian. At measurement times, each ensemble member is updated as

$$\mathrm{API}^{k,+}_{i,j} = \mathrm{API}^{k,-}_{i,j} + K_{i,j}(\mathrm{API}^{k,-}_{i,j} - \theta_{i,j} + \kappa^k_{i,j}), \tag{16}$$

where κ is sampled from a zero-mean Gaussian distribution with variance S. In the ENKF, K is calculated as a function of the ensemble variance of API$^-$ (CM) and measurement error covariance S:

$$K_{i,j} = \mathrm{CM}_{i,j}/(\mathrm{CM}_{i,j} + S_j), \tag{17}$$

and the analysis increment δ required in (9) is defined as

$$\delta_{i,j} = N^{-1}\sum_{k=1}^{N}(\mathrm{API}^{k,+}_{i,j} - \mathrm{API}^{k,-}_{i,j}). \tag{18}$$

[21] Despite the introduction of non-Gaussian error in the ENKF forecasting step, the update in (16) is still based on an implicit assumption of Gaussian error in API$^{k,-}$. Therefore, a complete treatment of non-Gaussian error requires the implementation of a PF. In a PF, individual ensemble members (or "particles") are assigned an initial weighting value W_k, where $W_k = N^{-1}$ and N now equals the number of total particles. Like the ENKF, the PF uses (16) to forecast the API value associated with each particle (API$^{k,-}_{i,j}$) until the first observation time. Upon the acquisition of an observation θ, the weights for each particle k are updated following

$$W^{k,+}_{i,j} = \frac{1}{\sqrt{2\pi S_j}}\exp\left[-\frac{(\mathrm{API}^{k,-}_{i,j} - \theta_{i,j})^2}{2S_j}\right]. \tag{19}$$

This updating is based on the (widely made) assumption that remotely sensed surface soil moisture retrievals have Gaussian errors [see, e.g., *Nagarajan et al.*, 2011]. Note that (19) leads to unequal weight for each particle and, if left unchecked, will eventually concentrate all weighting on a small number of particles. In order to redistribute weighting equally among all N particles and avoid this well-known degeneracy problem, the resampling algorithm described by *Liu and Chen* [1998] is applied. Their algorithms selects a new set of N particle values API$^{k,+}$ with equal weighting by, essentially, replicating particles with high $W^{k,+}$ and removing particles with low $W^{k,+}$. In this way the tendency for all weight to concentrate on a small number of particles is curbed, and the filter is made self-sustainable. Using this resampled set of API$^{k,+}$, δ is derived from (18), and the process is repeated for the next observation interval. Because the PF makes no parametric assumptions concerning the background error distribution of API forecasts, it should provide a superior filter for the case of non-Gaussian error in P'. Since the variance parameter Λ is largely unknown, ENKF and PF results will be presented for a range of possible choices.

3.5. Soil Moisture Modeling

[22] Another characteristic of the C09 baseline is its reliance on a simple soil moisture model. It is difficult to systematically examine the impact of alternative models since an almost infinite array of more complex (and more highly parameterized) soil moisture modeling approaches exist. As an alternative, we will focus on two fundamental differences between the API model and a more complex land surface model: (1) the API model lacks temporal variations in γ (i.e., soil water loss rate) associated with meteorological and/or radiation conditions, and (2) the API model lacks an explicit representation of maximum soil water capacity.

[23] In order to examine the impact of varying γ on the basis of meteorological conditions, daily average potential evaporation data (PET) and surface air temperature data (T_a) are obtained from an atmospheric reanalysis and are used to modify γ in (2) using either

$$\gamma'_{i,j} = \gamma_{i,j} - \Delta_{\mathrm{PET}}(\mathrm{PET}_{i,j} - \langle\mathrm{PET}\rangle_{D(i),j}) \tag{20}$$

or

$$\gamma'_{i,j} = \gamma_{i,j} - \Delta_{T_a}(T_{a,i,j} - \langle T_a\rangle_{D(i),j}), \tag{21}$$

where the angle brackets represent the climatological average of a given quantity within a 31 day, multiyear moving average window centered on day of year D. Both PET and T_a should be inversely correlated with γ (i.e., larger γ equates to more soil water retention, which in turn, is associated with low evapotranspiration, PET, and T_a conditions). The two constants Δ_{PET} (W^{-1} m^2) and Δ_{T_a} (K^{-1}) modulate the sensitivity of γ' to temporal anomalies in PET and T_a. Since the correct values of these constraints are unknown, a wide range of Δ_{PET} (W^{-1} m^2) and Δ_{T_a} (K^{-1}) will be examined for evidence that introducing PET- and/or T_a-based variations (or any magnitude) into γ is associated with improved rainfall correction.

[24] The impact of a finite surface layer capacity can be mimicked by setting an upper limit on API predictions obtained during either the KF forecasting step in (1) or the updating step in (3). Any API update or forecast exceeding this saturation capacity is then immediately reset to the capacity, and excess water is assumed to leave the modeled system through either recharge or runoff. It is important to note that enforcing such a nonlinear threshold might have important consequences on selecting the correct sequential filter since the PF and ENKF are both better suited to addressing the impact of nonlinear thresholds than the KF.

4. Data and Domains

[25] Remotely sensed surface soil moisture retrievals θ° are obtained from application of the single-channel retrieval algorithm to X band (10.6 GHz) Advanced Microwave Scanning Radiometer–EOS (AMSR-E) T_B data [*Jackson et al.*, 2010]. Surface soil moisture retrievals are acquired with a spatial resolution of about 40^2 km^2 and measurement frequency of 1–2 days at midlatitudes. Screening is performed to mask areas with snow cover and/or experiencing active rainfall. After screening, retrievals obtained from both ascending and descending overpasses between 1 July 2002 and 31 December 2009 are combined and aggregated to form a (near) daily, 1° latitude-longitude product. The θ_{SCAT} product used in (14) is based on scatterometer observations obtained from the European Space Radar (ERS-1 and ERS-2) measurements and application of the soil moisture retrieval algorithm described by *Naeimi et al.* [2009] between mid-2003 and May 2007.

[26] A number of different remotely sensed rainfall data sets are also used for P' in (1). The TMPA is computed retrospectively as the version 6 3B42 product. It combines multiple intercalibrated passive microwave estimates, microwave-calibrated thermal infrared (TIR) estimates, and monthly gauge data [*Huffman et al.*, 2007]. In real time, the combined passive microwave portion of the TMPA is computed experimentally as the 3B40RT product, and the combined microwave plus microwave-calibrated TIR estimates are computed as the 3B42RT product [*Huffman et al.*, 2007]. These real-time products differ from the version 6 3B42 product in only using microwave data, being real time, using a different microwave precipitation data set from the calibration standard, and having a heterogeneous computational record. In particular, the upgrade in February 2005 approximately doubled the inventory of microwave data previously used, switched from 5 day to 3 h recomputations of the microwave-TIR relationships, and significantly improved the microwave-TIR calibration procedure in cold-land regions. The data record starting in January 2009 employs additional satellite data types (thus offsetting the termination of older satellites) and uses a climatological calibration by month and location that approximately corrects the observed monthly biases between 3B42RT and the version 6 3B42 [*Huffman et al.*, 2010]. Note that 3B40RT is not recalibrated. All three products (TRMM 3B42, TRMM 3B40RT, and TRMM 3B42RT) are resampled to a daily, 1° latitude-longitude grid between 50°N and 50°S. Daily rainfall accumulation is defined as the total depth of rainfall between 12:00 and 12:00 UTC. However, for the soil moisture product we define that same day by a period shifted 12 h into the future (00:00 to 24:00 UTC). This 12 h shift is assumed to effectively capture the necessary delay between rainfall and the resulting soil moisture. Results will focus solely on the correction of 3 day rainfall accumulation products. Results by *Crow et al.* [2009] suggest that this approximates the finest temporal scale at which robust correction of rainfall is possible using AMSR-E soil moisture retrievals.

[27] Land-water masking is based on the Moderate Resolution Imaging Spectroradiometer (MODIS) MCD12C1 land cover classification product. Any 1° box containing more than 25% open water is permanently masked from the analysis. PET and T_a products required as input into (20) and (21) are acquired from the National Centers for Environmental Prediction (NCEP) Reanalysis 2. Four 6-hourly reanalysis predictions per day are averaged to obtain a single 12:00 to 12:00 UTC daily average and then resampled onto a 1° spatial grid.

[28] Three independent rainfall products are used for verification. CONUS results are verified on the basis of comparisons with NCEP's Climate Prediction Center (CPC) 1° unified rain gauge analysis product [*Higgins et al.*, 2002]. Over West Africa, verification is based on three 1° African Monsoon Multidisciplinary Analysis (AMMA [*Lebel et al.*, 2009]) supersites located in Benin, Mali, and Niger (Figure 1). A distributed rain gauge network, with 10 measurement sites in the Mali supersite and 40 measurement sites in the Benin and Niger supersites, has been established in each by the AMMA program [*Mougin et al.*, 2009; *Cappelaere et al.*, 2009]. Measurements from each individual rain gauge site are spatially aggregated up to the 1° supersite scale using block kriging [*Ali et al.*, 2003]. Finally, for quasi-global (50°S to 50°N) results, verification is based on the gauge-corrected TMPA 3B42 precipitation product described above.

5. Results

[29] Sections 5.1–5.3 describe the impact of modifications presented in section 3 on rainfall correction results within CONUS. Modifications leading to improved performance are gathered into a new algorithm called the Soil Moisture Analysis Rainfall Tool (SMART). Following its formal definition, SMART is applied within CONUS in section 5.5 and then evaluated outside CONUS for the first time in sections 5.6 and 5.7. Initial intercomparison results in sections 5.1, 5.2, and 5.3 are based on tuning the constant parameter λ in (9) to minimize the RMSE difference between SMART rainfall products and the benchmark CPC

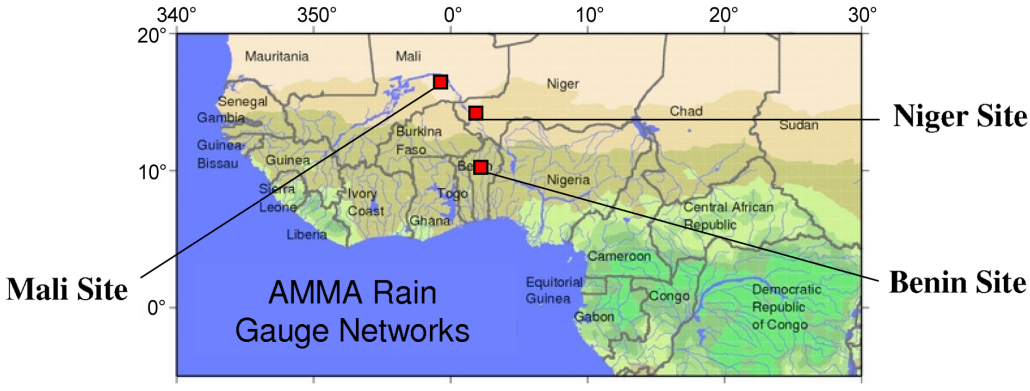

Figure 1. Location of the three West African African Monsoon Multidisciplinary Analysis (AMMA) supersites.

unified rain gauge analysis. However, SMART results in sections 5.6 and 5.7 will also examine the impact of simply assuming $\lambda = 0.60$. Since soil moisture retrievals have been screened to remove time periods with snow cover, accumulation results should be interpreted as reflecting only liquid precipitation conditions.

5.1. Impact of Filtering Modifications (R^2 and RMSE)

[30] For convenience, potential filtering modifications introduced in sections 3.1 to 3.3 are indicated by references to three incremental cases. Case 1 is the C09 baseline plus one of the alternative rescaling techniques presented in section 3.1, case 2 is case 1 plus the new error forecasting technique described in section 3.2, and case 3 is case 2 plus the alternative Q and S calibration approach introduced in section 3.3. For reference, these case definitions are also listed in Table 2.

[31] Figures 2 and 3 describe the performance of various satellite-based rainfall products over CONUS. As described in section 4, all results are based on comparisons between 1°, 3 day rainfall accumulations obtained from (original and corrected) satellite-based rainfall products with the CPC unified rain gauge data set between June 2002 and December 2009. Comparisons are performed separately for all 807 of the 1° grid boxes in CONUS and then spatially averaged to produce the results plotted in Figure 2. Uncorrected 3B40RT 3 day accumulations have a (CONUS-averaged) RMSE of 13.1 mm and an explained variance (i.e., square of Pearson's correlation coefficient R) of 0.32. Upon application of the baseline C09 algorithm, these values improve to 10.0 mm and 0.40, respectively.

[32] Figure 2 also depicts the added value of the modifications to the baseline C09 approach described in section 3.

Table 2. Variation in Case 3 RMSE and R^2 CONUS Results Associated With the Modification of ξ and Q Relative to the Baseline Values Listed in Table 1[a]

Constant	R^2	RMSE (mm)
Baseline (Table 1)	0.458	10.09
$\xi = 2$	0.458	10.12
$\xi = 10$	0.455	10.09
$Q = 1$ (mm^2)	0.455	10.25
$Q = 5$ (mm^2)	0.459	10.02

[a]CONUS, contiguous United States; RMSE, root-mean-square error.

Changing the soil moisture rescaling strategy from the static linear approach in (4) to the dynamic approach in (10) (to produce case 1) further improves the RMSE and R^2 of 3 day accumulation estimates to 9.7 mm and 0.43, respectively. While potentially requiring more historical data to parameterize, (10) allows climatological differences between API and $\theta°$ to be resolved before they impact (9). Somewhat surprisingly, none of the other alternative rescaling approaches discussed in section 3.1 display any obvious benefit. For example, allowing sampled σ statistics in (10) to vary seasonally leads to slightly worse rainfall accumulation estimates, and the nonlinear CDF-matching transformation in (11) produces significantly poorer results for the cases of both a single bulk transformation and the application of separate transformations applied within each 31 day

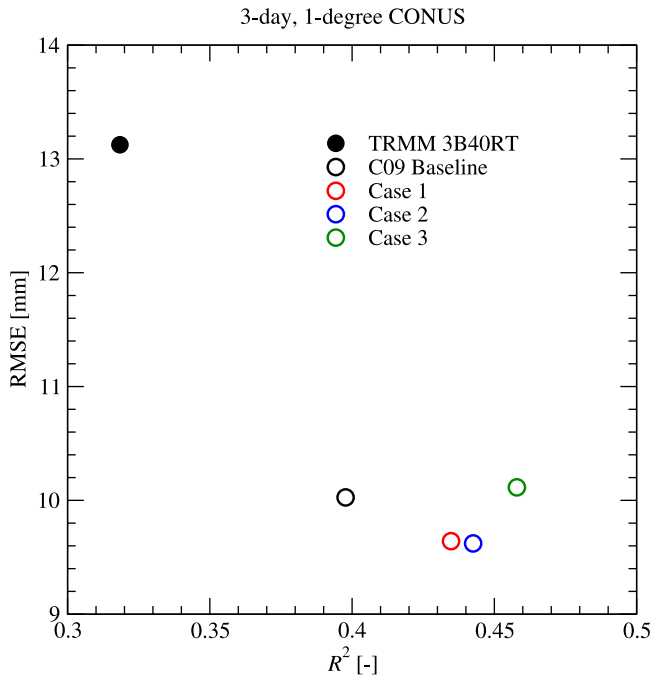

Figure 2. Contiguous United States (CONUS)-averaged root-mean-square error (RMSE) and R^2 for 3 day, 1° 3B40RT accumulations and corrected accumulations using both the C09 baseline and the three modified cases described in Table 2.

seasonal window (not shown). However, care should probably be taken when broadly interpreting these results. Difficulties with CDF matching may arise from our particular focus on rainfall accumulation correction (as opposed to the more common data assimilation goal of correcting soil moisture) and sampling issues associated with parameterizing (11) using only 7.5 years of historical data. Nevertheless, all subsequent references to case 1 will refer only to the application of (10).

[33] Adding the conditioning of rainfall error via (12) (to produce case 2) leads to incremental R^2 and RMSE improvements relative to case 1 (Figure 2). Such conditioning allows the filter to adjust the background error variance in response to recently observed rainfall amounts and to make more informed decisions regarding the appropriate weighting of new observations. Note that both cases 1 and 2 calibrate Q and R using a consistent ν-whitening approach (see section 3.3). As a result, the differences noted between case 1 performance and case 2 performance can be attributed directly to the introduction of nonzero ξ in (12). In contrast, case 3 drops ν whitening altogether and instead estimates S on the basis of the TC approach described in section 3.3. This change improves case 3 R^2 results relative to case 2.

[34] In summary, moving between cases 1, 2, and 3 in Figure 2 produces continual improvement in rainfall R^2 with gauge data. However, the transition between cases 2 and 3 is also associated with a slight increase in rainfall accumulation RMSE. An additional consideration is that the implementation of cases 2 and 3 requires the additional parameter ξ and the outside specification of Q (previously fixed via ν whitening in C09 and case 1; Table 1). However, a preliminary sensitivity analysis suggests that case 3 performance is relatively insensitive to both parameters (Table 3). The lack of sensitivity to Q is not surprising since during high-precipitation periods most of the API forecast covariance T^- is now created by the $\xi P'^2$ term in (12), with the Q term assuming a secondary role. Likewise, the lack of sensitivity to ξ would seem to indicate that even a low value of ξ produces sufficiently high T^- in (12) to produce essentially direct insertion conditions for the Kalman filter (i.e., $K = 1$) during periods of significant rainfall. Whatever the cause of this insensitivity, Table 3 suggests that even a rough parameterization of ξ and Q is adequate for good case 3 performance.

[35] Improvements in rainfall accuracy noted in Figure 2 also vary spatially with land cover type. Over CONUS, Figure 3 plots 1° changes in RMSE and R^2 realized upon application of the C09, case 1, case 2, and case 3 algorithms. Within heavily vegetated areas the C09 baseline demonstrates no net R^2 improvement (and even modest degradation). However, steady incremental improvement (i.e., higher R^2) is associated with the implementation of all three modified cases, with the largest improvements occurring between C09 and case 1 in the Pacific Northwest and cases 2 and 3 in eastern CONUS (Figure 3). As noted above, the transition between cases 2 and 3 is also associated with a slight CONUS-wide increase in RMSE.

Table 3. Incremental Filtering Modification Cases

Case Name	Description
C09	*Crow et al.* [2009] baseline
Case 1	C09 plus soil moisture rescaling modification in (10)
Case 2	Case 1 plus background error forecasting modification in (12)
Case 3	Case 2 plus filter calibration modification in (14)

5.2. Impact of Filtering Modifications (Categorical Measures)

[36] Figure 4 provides an alternative evaluation of cases 1, 2, and 3 using nonparametric categorical measures based on defining a storm "event" as 3 day rainfall accumulations in excess of a given threshold. Defining H to be the number of such events successfully predicted by a given rainfall product (out of N_E total events), F to be the number of nonevents erroneously predicted, and M to be the number of actual events that were missed, the false alarm ratio (FAR), probability of detection (POD), and threat score (TS) are defined as

$$\mathrm{FAR} = \frac{F}{H+F}, \tag{22}$$

$$\mathrm{POD} = \frac{H}{H+M}, \tag{23}$$

$$\mathrm{TS} = \frac{H}{H+F+M}. \tag{24}$$

A perfect accumulation time series yields FAR = 0, POD = 1, and TS = 1. Note that TS provides an integrated measure of categorical performance that is sensitive to both the probability that a given event is detected and the probability that a predicted event occurs.

[37] These metrics can be calculated for a range of 3 day accumulation thresholds used to define a storm event. Figure 4 shows changes in FAR, POD, and TS upon implementation of the C09, case 1, case 2, and case 3 algorithms. As before, accumulation values obtained from the CPC unified rain gauge analysis are used as benchmark truth. For each 1° CONUS box, all 3 day periods with a (CPC-based) cumulative rainfall accumulation of 2 mm or greater are ranked according to their 3 day accumulation total. Note that the 2 mm baseline is motivated by known deficiencies in the quality of CPC rain and no-rain predictions at low accumulation thresholds [*Janowiak et al.*, 2004]. Using this ranked list of 3 day accumulation totals, threshold percentiles on the x axis of Figure 4 are translated into a specific 3 day rainfall accumulation threshold for each 1° CONUS box. Results plotted in Figure 4 represent the CONUS-wide average for the change in 3B40RT FAR, POD, and TS metrics for an event threshold defined by each percentile level.

[38] The use of CONUS-wide averages provides a relatively stringent test since it forces various approaches to attempt rainfall correction over a wide range of land cover classes, many of which are ill suited for soil moisture remote sensing at the X band (10.6 GHz) [*Njoku et al.*, 2003]. Partly as a consequence, two problems are evident in categorical results for the C09 baseline algorithm presented in Figure 4 (black lines). First, the application of the C09 algorithm tends to reduce the probability that very

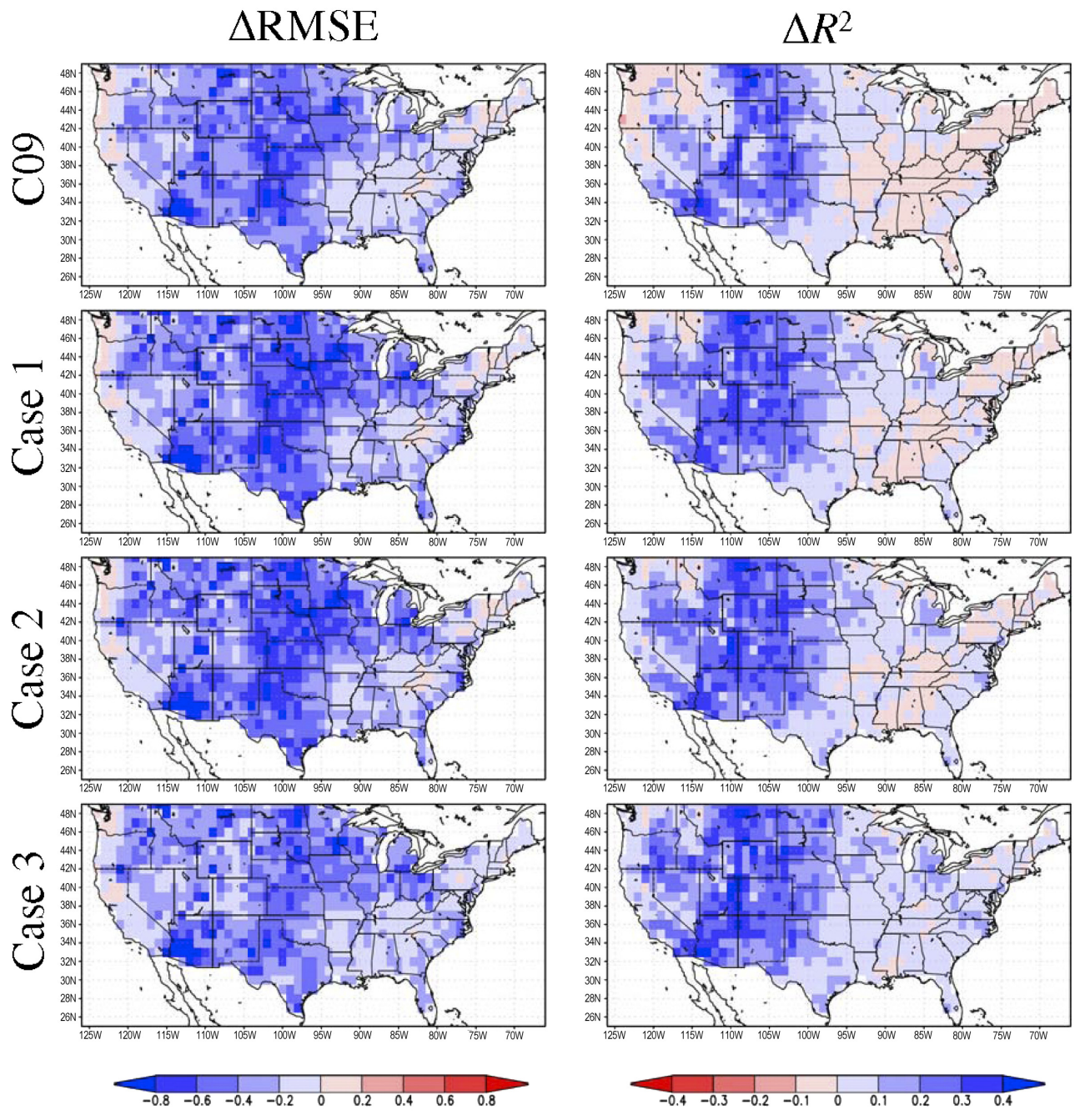

Figure 3. Improvement in 3B40RT RMSE and R^2 (3 day accumulations) for the C09 baseline, case 1, case 2, and case 3 algorithms. Note that Δ RMSE is normalized by the uncorrected 3B40RT RMSE in each 1° grid box to create a unitless variable. The color bar is constructed so that blue (red) shading always indicates improvement (degradation) relative to the uncorrected 3B40RT product.

large events will be detected (i.e., it produces negative ΔPOD for threshold percentiles greater then 80% in Figure 4b). Conversely, the C09 algorithm overestimates the frequency of low-intensity rainfall events (i.e., it produces positive ΔFAR for threshold percentiles less than 50% in Figure 4a). POD problems at high accumulation thresholds are likely an inherent problem with any soil moisture-based correction scheme. Large events typically produce more rainfall than is needed to saturate surface soil moisture levels. Consequently, their magnitude cannot be unambiguously inferred from subsequent soil moisture dynamics. As a result of this saturation effect, the C09 algorithm tends to be overly skeptical of high-intensity events in the 3B40RT data set and is too aggressive in correcting them back to lower accumulation amounts. While this skeptical bias aids in reducing FAR, it also harms POD for high-threshold events. Conversely, FAR problems at low thresholds occur primarily when positive temporal trends in θ° caused by retrieval error noise are misidentified as low-intensity rainfall events.

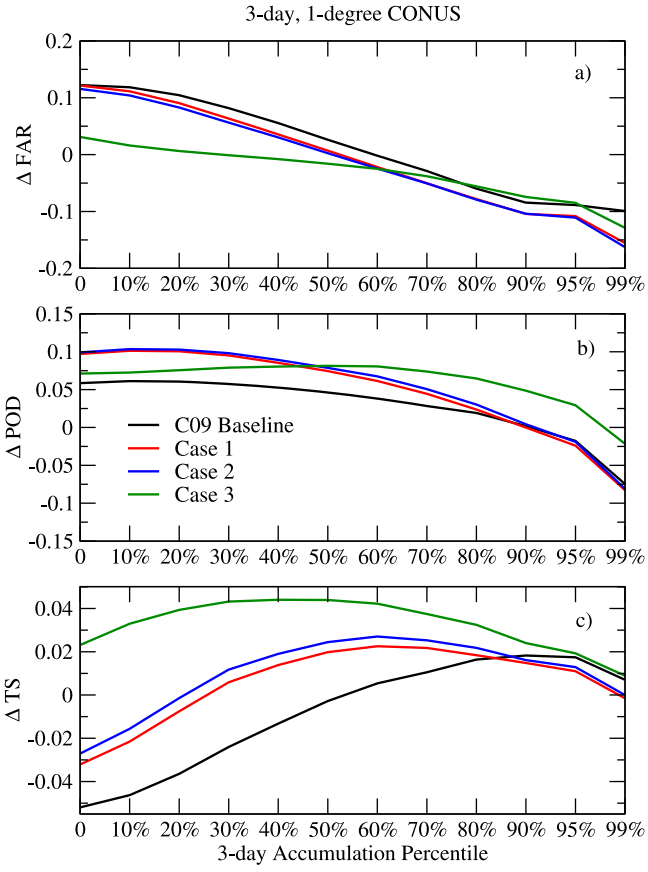

Figure 4. Change in (a) false alarm ratio (FAR), (b) probability of detection (POD), and (c) threat score (TS) for the C09 baseline, case 1, case 2, and case 3 algorithms and a range of 3 day accumulation thresholds.

[39] As a result of these shortcomings, the C09 algorithm fails to uniformly improve TS for all event thresholds (Figure 4c). While the complete elimination of both low-threshold POD and high-threshold FAR problems is difficult, both shortcomings can be progressively minimized by implementing the filtering modifications described in section 3. In particular, case 3 results show simultaneous improvement to both FAR results at low thresholds (Figure 4a) and POD problems at high thresholds (Figure 4b). As a result, it succeeds in improving TS across the entire range of thresholds examined in Figure 4. Qualitatively similar improvements are seen when TS is replaced with either the equitable threat score [*Mason*, 2003] or the hit rate (H/N_E) categorical metric.

5.3. Additional Filtering Modifications

[40] However, not all potential filtering modifications to the C09 baseline approach lead to improved accumulation predictions. Section 3.3 describes alternative ENKF- and PF-based correction approaches that allow rainfall errors to be generated via multiplicative perturbations sampled from a lognormal distribution (as opposed to the additive, Gaussian basis of the C09 baseline algorithm). In Figure 5 (as in Figure 2), uncorrected 3B40RT products are associated with relatively large 3 day accumulation errors (black circle). A substantial fraction of this error is removed by applying the KF-based case 3 algorithm. Figure 5 also shows the impact of swapping out the KF core of case 3 and replacing it with either a PF or ENKF capable of capturing multiplicative rainfall errors (see section 3.4). Here ensemble size (N) is set equal to 2000, and a range of choices for Λ in (15) are tested. A large value of N is intentionally chosen to insulate PF and ENKF results against ensemble sampling errors. Nevertheless, no added benefit is associated with either the PF or ENKF modification for any reasonable choice of Λ. This suggests that at the relatively coarse time and space scales considered here (3 day and 1°), there is no benefit in replacing the Gaussian error model at the core of the C09 algorithm.

[41] A final filtering simplification in C09 is the exclusive reliance on a one-dimensional filtering approach whereby rainfall accumulations in a given grid box are updated only via $\theta°$ retrievals in that particular box and no consideration is paid to the lateral (i.e., grid box to grid box) transfer of information. In order to quantify the potential value of retrievals in neighboring grid boxes, a test case was constructed in which the analysis increments additively applied to rainfall (i.e., δ in (9)) were calculated using a weighted average of analysis increments for a central 1° grid box (spatially corresponding to the rainfall time series being corrected) as well as increments calculated for the eight grid boxes immediately surrounding it. Despite applying a wide variety of relative weights to these surrounding grid boxes, this modification did not produce a discernible improvement relative to the C09 baseline case of placing all weight on analysis increments calculated for the center 1° grid box (not shown). This result implies that

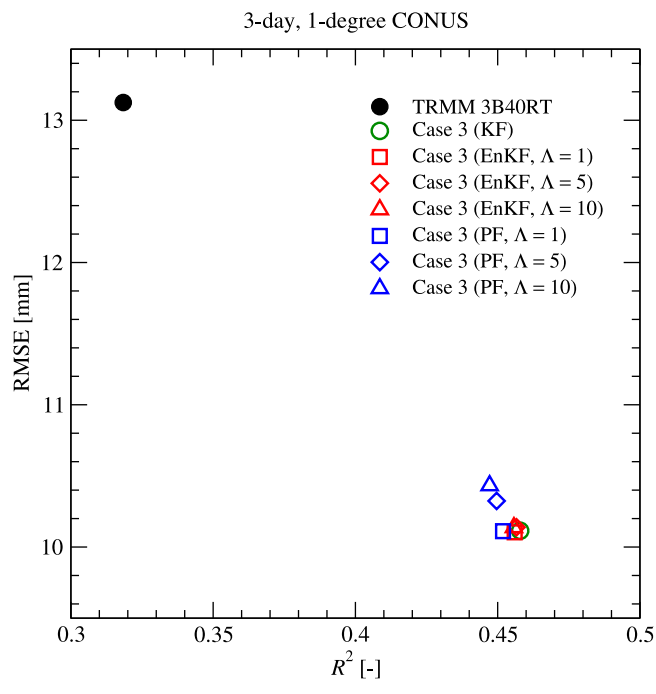

Figure 5. CONUS-averaged RMSE and R^2 for 3 day 3B40RT accumulations and case 3–corrected accumulations based on a Kalman filter (KF), ensemble Kalman filter (ENKF), and particle filter (PF) implementation of case 3 (and various choices of Λ).

one-dimensional data assimilation approaches are adequate at 1° spatial resolution.

5.4. Impact of Modeling Modifications

[42] The baseline C09 rainfall correction algorithm also utilizes a simple soil moisture forecasting model. The physical realism of the model should impact the accuracy of the rainfall correction approach. For instance, errors associated with the inaccurate modeling of evapotranspiration should ideally be minimized (or compensated for) before they are misattributed to rainfall uncertainty. Given the known dependence of evapotranspiration on air temperature (T_a) and PET, the alternative parameterization of γ' presented in (20) and (21), which explicitly take into account T_a and PET variations, should aid in the modeling of soil moisture dynamics. In both equations, the sensitivity of γ' to T_a and PET temporal anomalies is controlled by a single parameter (Δ_{PET} or Δ_{T_a}). Values of zero for these sensitivity parameters cause the parameterization of γ' to fall back on (2). Increasing Δ_{PET} or Δ_{T_a} gradually enhances the amount of influence that PET and T_a anomalies have on γ' and thus the API time series that forms the basis of the rainfall correction approach. For the case 3 algorithm, Figure 6 describes the impact of Δ_{PET} and Δ_{T_a} on the net improvement of corrected rainfall R^2 versus the CPC unified benchmark. In contrast to expectations, nonzero values of Δ_{T_a} and Δ_{PET} are associated with a general reduction in R^2 improvement. Consequently, no added value is associated with the inclusion of T_a and PET anomaly information in (2).

[43] A second change associated with a more complex land surface model is the imposition of a maximum soil water capacity on modeled soil moisture values (in contrast to the unbounded API model in (1)). Figure 7 examines the impact of such limits on the performance of the case 3 algorithm. As in Figure 6, 3 day rainfall accumulation predictions are evaluated on the basis of their R^2 fit to the CPC unified rain gauge analysis. Note that the imposition of any finite storage capacity in Figure 7 is associated with degraded algorithm performance. The imposition of a maximum capacity results in periods of soil water saturation and the subsequent loss of antecedent rainfall information in API forecasts. These results suggest that the degrading effect of saturation information loss outweighs the benefits of obtaining a soil moisture time series that realistically reflects actual soil saturation effects. Similar results are found for the use of both a PF and an ENKF despite that fact that the PF is better equipped to handle the nonlinearity imposed by a finite soil water capacity.

[44] The modeling changes discussed above are admittedly somewhat ad hoc and have not been independently verified to improve soil moisture predictions. Consequently, Figures 6 and 7 cannot be interpreted to suggest that (1) is optimal. However, these results suggest that fundamental processes that a more complex soil moisture model would add to (1) (i.e., energy balance control on soil water loss via (20) and (21) and soil saturation and runoff generation) do not necessarily enhance the correction of rainfall accumulations.

5.5. SMART Implementation in CONUS

[45] Hereinafter, case 3 (i.e., the one-dimensional KF approach of C09 with the three modifications introduced in sections 3.1, 3.2, and 3.3) is referred to as the Soil Moisture Analysis Rainfall Tool (SMART). Required SMART parameters and their assigned values are listed in Table 1. Note that the alternative use of the ENKF and/or PF (described in section 3.4) and the modeling modifications described in section 3.5 are not implemented.

[46] Two factors impacting the additive skill associated with SMART are the accuracy of uncorrected precipitation

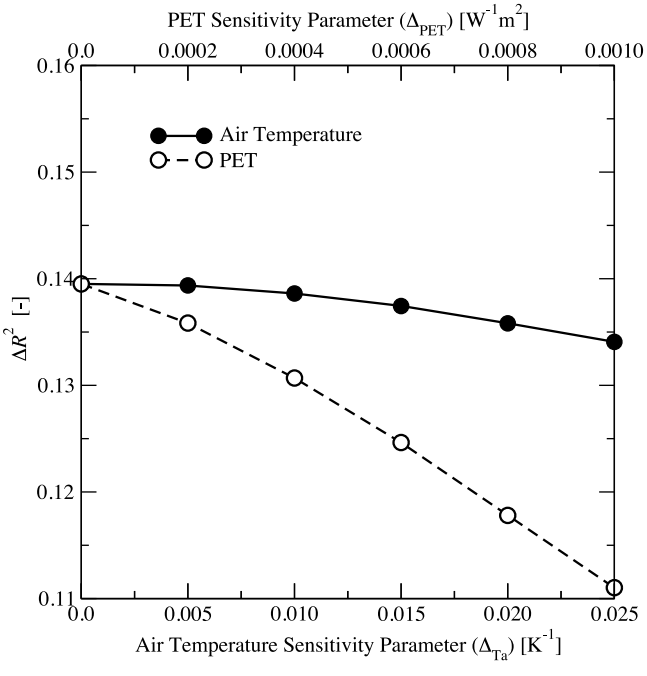

Figure 6. The improvement of CONUS-averaged R^2 (ΔR^2) for case 3 results derived with various levels of Δ_{PET} and Δ_{T_a}.

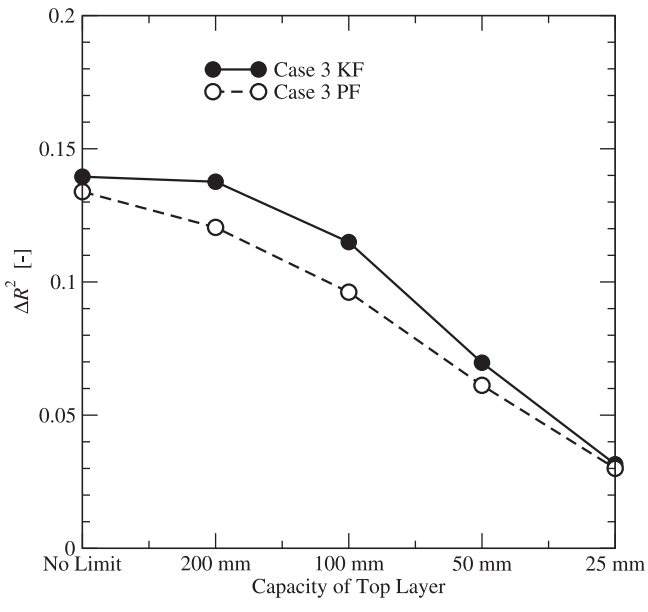

Figure 7. The improvement of CONUS-averaged R^2 (ΔR^2) for case 3 results derived using various maximum antecedent precipitation index (API) capacities. Results are shown for both the ENKF and PF cases.

products and the information assumed to be available for the calibration of λ in (9). With regard to the first point, it should be stressed that the two real-time TMPA products examined here (3B40RT and 3B42RT) are not based on historically constant methodologies [*Huffman et al.*, 2010]. In particular, two significant changes have modified the TMPA real-time product generator: the significant expansion of input microwave observations in February 2005 and the modification of the real-time TMPA calibration procedure in January 2009 (see section 4 for further details). No TMPA reprocessing of past real-time products was attempted in either case. Table 4 uses these two key events to divide the entire 2002–2009 analysis into three separate time periods: August 2002 to January 2005, February 2005 to December 2008, and January 2009 to December 2009. General improvement in the accuracy of both real-time TMPA products is noted between different periods as methodological advances improve the accuracy of TMPA products. This improvement in uncorrected TMPA rain accumulation products is also associated with a steady decline in the additive value of SMART corrections. That is, smaller amounts of added value are noted as the underlying TMPA rain products improve. This trend illustrates both the competitive relationship between soil moisture and precipitation retrievals in the SMART analysis and the enhanced value of SMART for locations where existing rainfall products are poor.

[47] In addition, all results to this point have been based on tuning the constant, dimensionless parameter λ in (9) to minimize the long-term RMSE difference between SMART rainfall products and the benchmark CPC unified rain gauge analysis. Since it presumes the retrospective availability of relatively good daily rain gauge data, this "optimal λ" strategy may be difficult to implement in data-poor areas. As a way forward, *Crow et al.* [2009] suggest two additional strategies: (1) calibrating λ against an independent rainfall data set or (2) setting λ to a globally constant value. While the first strategy tends to yield slightly better results [*Crow et al.*, 2009], finding truly independent global precipitation products is difficult; therefore, results here will focus on the second strategy of simply fixing $\lambda = 0.60$. Figure 8 describes the impact of this approach on the application of the SMART algorithm to the 3B40RT, 3B42RT, and 3B42 rainfall products within CONUS. Uncorrected products are indicated with solid black symbols, and SMART-corrected rainfall utilizing optimal λ are indicated using open black symbols. Gray symbols in Figure 8 show results for the blanket assumption that $\lambda = 0.60$. Relative to the use of an RMSE-optimal λ, this assumption produces only marginally worse results, and substantial improvement relative to uncorrected TMPA products is still observed (Figure 8).

Table 4. Impact of TMPA Real-Time Historical Processing Changes on 3B40RT and 3B42RT Accuracy and the Magnitude of Improvement Associated with SMART[a]

Product	Time Period	R^2	R^2 With SMART	ΔR^2
3B40RT	Aug 2002 to Jan 2005	0.267	0.418	0.152
	Feb 2005 to Dec 2008	0.386	0.494	0.108
	Jan 2009 to Dec 2009	0.453	0.531	0.079
3B42RT	Aug 2002 to Jan 2005	0.337	0.465	0.128
	Feb 2005 to Dec 2008	0.458	0.550	0.092
	Jan 2009 to Dec 2009	0.450	0.540	0.089

[a]All values are for 3 day, 1° accumulations within CONUS. TMPA, Tropical Rainfall Measuring Mission (TRMM) Multisatellite Precipitation Analysis.

[48] A valuable point of reference for improvement in rainfall accumulation estimates associated with SMART are comparable improvements realized upon the incorporation of other types of observational data. As described in section 4, the TMPA system generates a cascade of products in which a progressively wider range of observation types are collectively applied to estimate rainfall accumulations [*Huffman et al.*, 2007]. The 3B40RT product represents a baseline of using only microwave-based products, while 3B42RT captures the incremental value associated with also integrating TIR remote sensing observations. Likewise, the 3B42 product captures improvements arising from the use of rain gauge data to bias correct 3B42RT accumulation estimates on a monthly scale. Within CONUS, the incremental value of incorporating this cascade of observation types is reflected in the consistent improvement of RMSE and R^2 metrics for the 3B40RT, 3B42RT, and 3B42 products versus the CPC benchmark (see solid black symbols in Figure 8). Comparable improvements can also be realized by applying the SMART algorithm. In particular, within the CONUS domain, results for applying the SMART algorithm to the 3 day 3B40RT "microwave-only" product are substantially better, in both a RMSE and R^2 sense, than results for the uncorrected, 3 day 3B42RT "microwave-TIR" product. That is, on average within CONUS, soil moisture information contributes more to 3 day, 1° TMPA rainfall estimates than the introduction of TIR remote sensing information. Applying the SMART algorithm to the uncorrected 3B42RT microwave-TIR product also leads to enhanced rainfall accumulation predictions; however, because of high rain gauge densities in CONUS, SMART-corrected 3B42RT results cannot match the accuracy of the 3B42 "microwave–TIR–rain gauge" product for 3 day accumulations. Consequently, in densely instrumented areas like CONUS, the added value of SMART lags that provided by monthly rain gauge data.

5.6. Smart Implementation in West Africa

[49] To date, all results (for either SMART or its C09 precursor) have been for locations within CONUS. While the availability of the CPC unified rain gauge data set makes CONUS a good test bed site for SMART, results there do not speak directly to the operational implementation of SMART in data-poor areas of the world where soil moisture observations are likely to have the largest positive impact on rainfall accumulation estimates. Rainfall data collected during the West African AMMA experiment provides an opportunity to assess SMART performance in one such region.

[50] After 2002, ERS scatterometer soil moisture observations are not widely available outside of CONUS and Europe. This prevents the application of (14) to estimate S. Therefore, for the AMMA and quasi-global analysis (section 5.7) we estimate S on the basis of monthly enhanced vegetation index (EVI) measurements taken from the monthly MODIS MYD13C2 product:

$$S_{i,j} = \left(\frac{\sigma_j^{\mathrm{API}}}{5\sigma_j^{\theta}} \mathrm{EVI}_{i,j} \right)^2 . \tag{25}$$

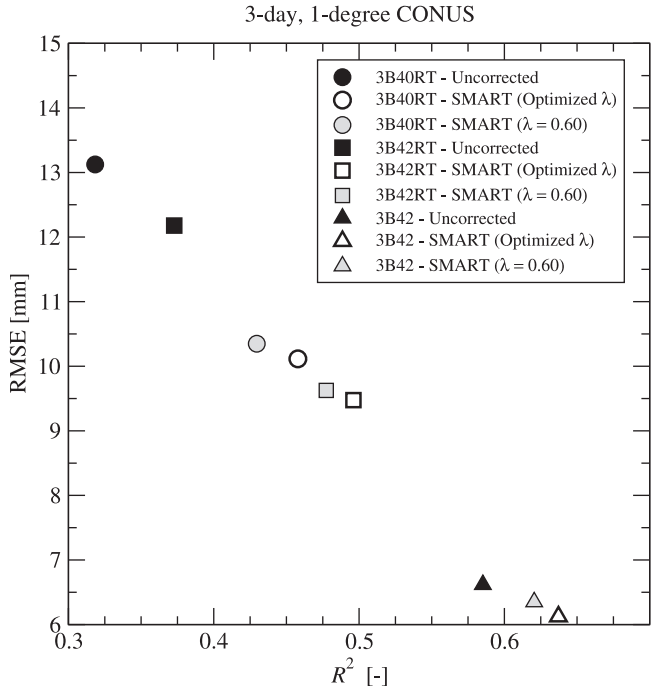

Figure 8. CONUS-averaged RMSE and R^2 for case 3–corrected 3 day accumulations associated with various Tropical Rainfall Measuring Mission (TRMM) Multisatellite Precipitation Analysis (TMPA) products and λ strategies.

This parameterization recognizes the first-order importance of biomass amount, characterized using EVI, on the level of error in $\theta°$. As a consequence, larger S, and therefore less weight on θ retrievals, is specified for heavily vegetated land surfaces.

[51] Table 5 summarizes SMART results for correction of the TRMM 3B40RT product in AMMA supersites over Benin, Niger, and Mali shown in Figure 1 using an optimal λ approach. Results correspond to the June 2002 through 2009 time period for Benin and Niger and the May 2005 through 2009 period for Mali. SMART is able to improve 3 day accumulation RMSE and R^2 over all three supersites. However, as noted above in section 2, it has no impact on long-term biases at each site. Figure 9 examines the impact of alternative rain products and λ estimation techniques by replicating Figure 8 except that CONUS-wide averages are now replaced by analogous averages obtained at three AMMA supersites.

[52] As in CONUS (Figure 8), the alternative strategy of fixing $\lambda = 0.60$ slightly underperforms the explicit optimization of λ, and SMART-corrected 3B40RT "microwave-only" results are close to the uncorrected 3B42RT microwave-TIR product in terms of RMSE and R^2. This equivalence suggests that on average among the AMMA supersites, soil moisture information contributes as much information to coarse-scale rainfall accumulation estimates as TIR remote sensing. In addition, because of sparse rain gauge coverage in West Africa, SMART-corrected 3B42RT microwave-TIR results outperform the 3B42 microwave–TIR–rain gauge product in terms of R^2 fit to AMMA rain gauges. Therefore, over West Africa at 3 day, 1° resolutions, soil moisture data provide as much information as satellite-based TIR measurements and, at least for R^2-based evaluations, more information than sparse rain gauge data ingested by the 3B42 product in the region. However, SMART-based corrections still lag in terms of RMSE correction because of long-term biases in the TRMM 3B42RT product that are corrected via rain gauge comparisons but neglected by SMART (Table 5).

5.7. Quasi-global SMART Algorithm Implementation

[53] Verification of SMART results in areas lacking extensive rain gauge data is difficult, but a preliminary analysis is possible using the TMPA 3B42 product as a source of ground truth. Here SMART is evaluated on the basis of its ability to correct real-time, satellite-only 3B40RT accumulations to more closely resemble the retrospective, gauge-corrected 3B42 product. Figure 10 illustrates such comparisons by plotting the impact on RMSE and R^2 for 3 day 3B40RT accumulation estimates between 50°S and 50°N. Figure 10 (top) shows results based on the optimization of λ assuming the availability of the entire 3B42 retrospective data set. Since such historical data may not be available in many operational circumstances, Figure

Table 5. Impact of Applying SMART to the Correction of 3 Day TRMM 3B40RT Rainfall Accumulation Products Over the Three AMMA Supersites in Figure 1[a]

Site	Product	R^2	RMSE (mm)	Bias (mm)
Mali	3B40RT	0.286	11.89	2.22
	3B40RT + SMART	0.489	9.23	2.22
Niger	3B40RT	0.284	21.77	5.79
	3B40RT + SMART	0.414	16.15	5.79
Benin	3B40RT	0.510	16.77	4.75
	3B40RT + SMART	0.573	14.63	4.75

[a]AMMA, African Monsoon Multidisciplinary Analysis.

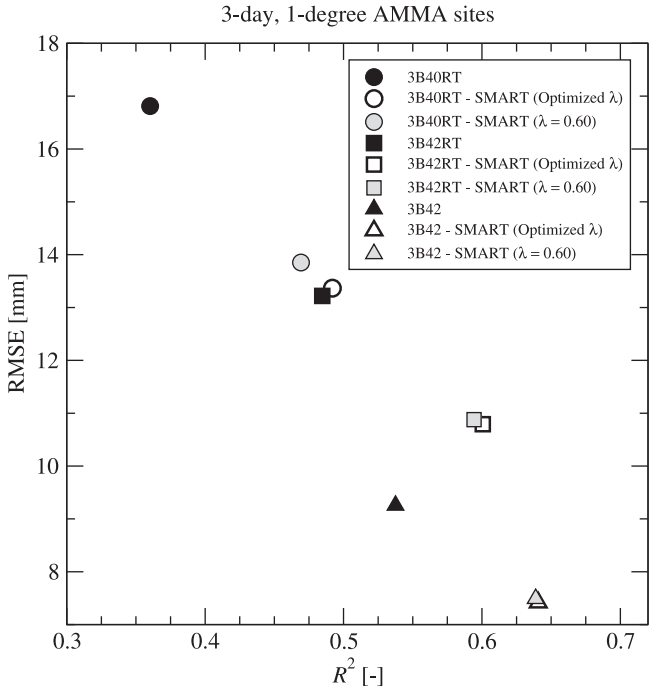

Figure 9. AMMA site-averaged RMSE and R^2 for case 3–corrected 3 day accumulations associated with various TMPA products and λ strategies.

10 (bottom) show similar results obtained for the fixed $\lambda = 0.60$ case. Regardless of the method applied to estimating λ, relative RMSE changes demonstrate almost uniform improvement. While large R^2 improvement is generally limited to lightly vegetated areas (e.g., the western United States, the Iberian Peninsula, the Middle East, and Australia), even densely vegetated areas show either small improvements or no net change.

[54] It is worth noting the impact of uncertainty in the 3B42 product used as the benchmark in Figure 10. When

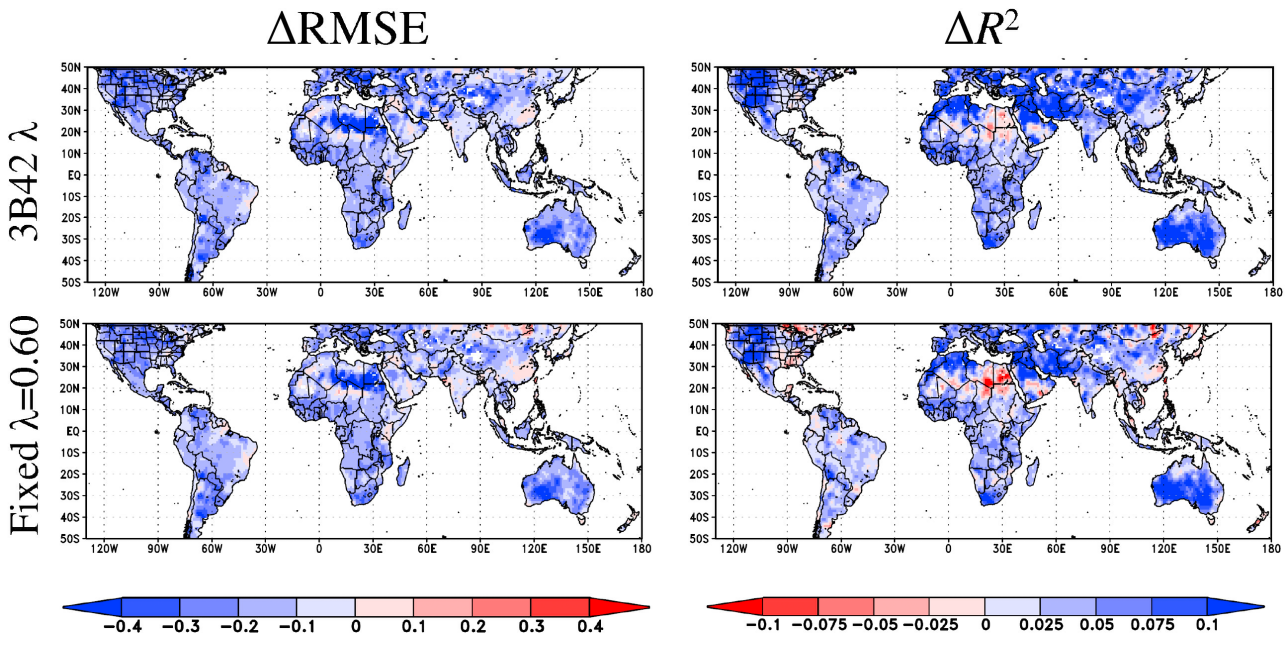

Figure 10. Quasi-global impact of SMART on the correction of 3 day 3B40RT accumulation products relative to 3B42. Results are shown for the estimation of λ using fitting against both 3B42 and the fixed case of $\lambda = 0.60$. Δ RMSE is normalized by the uncorrected 3B40RT RMSE, and the color bar is constructed so that blue (red) shading always indicates improvement (degradation) relative to the uncorrected 3B40RT product.

results are averaged across all three AMMA supersites, application of SMART to the 3B40RT data set improves the R^2 fit of 3 day accumulations to the AMMA baseline (for the optimal λ case) by about 0.13 (Figure 9). Changing only the benchmark rain gauge data from AMMA rain gauge observations to the lower-quality 3B42 product reduces the apparent R^2 improvement to less than 0.01. This reduction suggests that our ability to observe incremental improvement associated with SMART is partially dependent on the availability of relatively accurate benchmark rain gauge observations for evaluation. Therefore, in poorly instrumented areas of the world, the improvements seen in Figure 10 are likely conservative (i.e., larger improvements would likely be noted if higher-quality reference data were available for verification).

6. Summary and Conclusions

[55] This analysis improves upon the rainfall correction algorithm presented by *Crow et al.* [2009] and broadens its application to areas outside of CONUS. Specific modifications made to the soil moisture scaling (section 3.1), rainfall error parameterization (section 3.2), and filter calibration (section 3.3) components of the core data assimilation system led to substantial improvements in the ability of the algorithm to correct coarse-scale rainfall accumulation products (Figures 2, 3, and 4). However, no improvement was associated with the incorporation of non-Gaussian rainfall errors and/or the application of ENKF and PF sequential filters (Figure 5). In addition, prospects for improving corrections using a more complex land surface model are uncertain given the lack of apparent value for more complex evapotranspiration modeling approaches (Figure 6) and challenges associated with basing the algorithm on a multilayered model with finite soil water capacities (Figure 7).

[56] On the basis of these results, the optimal set of modifications identified in Figures 2–7 were formalized into the Soil Moisture Analysis Rainfall Tool (SMART) and applied to TMPA data products within CONUS and AMMA West African super-sites. For both locations, coarse-scale rainfall accumulation improvements associated with SMART implementation were shown to be as large, if not larger than, comparable improvements based on the integration of TIR satellite observations into a multisatellite rainfall product (Figures 8 and 9). In addition, for sparsely gauged regions of West Africa, SMART provides more R^2 correction than reprocessing to match monthly rain gauge totals (Figure 9). It should be stressed that these assertions of relative value are valid only for the particular spatial and temporal scales examined here (3 days and 1°). TIR satellite products, for instance, would almost certainly have greater relative value if rainfall accumulation estimates were evaluated at finer spatial and temporal scales. Nevertheless, these results demonstrate that remotely sensed surface soil moisture sensors should be considered a viable input into multisensor precipitation data products based on a backbone of TRMM or GPM observations. When applied at a quasi-global domain between 50°S and 50°N, SMART offers nearly uniform improvement to real-time TMPA rainfall products (Figure 10).

[57] Despite the methodological advances presented here, a number of other potential approaches exist to incorporate soil moisture information into rainfall estimates. For instance, *Pellarin et al.* [2009] report good results over West Africa using a data assimilation system to tune event-scale multiplicative factors for satellite-based rainfall accumulations so that C band (6.9 GHz) T_B predictions made by a simple water balance model and microwave emission algorithm match observed T_B. Relatively little is known about the relative benefits of SMART versus such an approach. It is also worth considering how results in Figure 7 (which demonstrate the degrading impact of imposing a finite soil capacity) might vary when (1) is replaced by a more complex, multilayer land surface model. In a multilayer soil water balance model, antecedent rainfall information is not strictly lost during periods of surface saturation but rather transferred into either surface runoff or drainage flux. Therefore, some additional benefit could be gained by implementing the flux correction algorithm of *Pan and Wood* [2007] to explicitly update runoff (in addition to soil moisture states) in more complex land surface models. Likewise, our approach for conditioning API with uncertain precipitation estimates (section 3.2) remains relatively simple and may benefit from existing approaches for generating realistic stochastic rainfall replicates conditioned on satellite observations [e.g., *Wojcik et al.*, 2009]. Finally, while preliminary evidence (see section 5.3) suggests that it does not lead to large improvements, the implementation of two-dimensional filtering approaches has not been fully explored. Future work should be aimed at exploring these issues and possibilities.

[58] The amount of improvement associated with soil moisture–based corrections is directly proportional to the accuracy of soil moisture retrievals and inversely proportional to the accuracy of the precipitation product being corrected (see, e.g., Table 4). Satellite-based precipitation estimates are expected to become significantly more accurate as the deployment of the GPM constellation unfolds. Likewise, the future use of low-frequency SMAP (and/or the European Space Agency Soil Moisture Ocean Salinity Mission) L band (1.4 GHz) observations, as opposed to X (10.6 GHz) and C band (6.9 GHz) observations available from current satellite sensors, will minimize the degrading effect of both atmospheric and vegetation canopy water on soil moisture retrievals and extend the range of circumstances under which retrievals can be accurately obtained [*Kerr et al.*, 2001]. Consequently, future trends in the additive value of SMART will likely be based on the interplay between these two accuracy trends.

[59] **Acknowledgments.** Support for this study was provided by the NASA Precipitation Measurement Missions Program through a grant to W. T. Crow. On the basis of a French initiative, AMMA was built by an international scientific group and is currently funded by a large number of agencies, especially from France, the United Kingdom, the United States, and Africa.

References

Ali, A., T. Lebel, and A. Amani (2003), Invariance in the spatial structure of Sahelian rain fields at climatological scales, *J. Hydrometeorol.*, *4*, 996–1011.

Bennartz, R., and G. W. Petty (2001), The sensitivity of microwave remote sensing observations of precipitation to ice particle size distributions, *J. Appl. Meteorol.*, *40*, 345–364.

Bytheway, J. L., and C. Kummerow (2010), A physical based screen for precipitation over complex surface using passive microwave observations, *IEEE Trans. Geosci. Remote Sens.*, *48*, 299–313.

Cappelaere, B., et al. (2009), The AMMA-CATCH experiment in the cultivated Sahelian area of south-west Niger: Strategy, implementation, site description, main results, *J. Hydrol.*, *375*(1–2), 34–51.

Clark, M., S. Gangopadhyay, L. Hay, B. Rajagopalan, and R. Wilby (2004), Schaake shuffle: A method for reconstructing space-time variability in forecasted precipitation and temperature fields, *J. Hydrometeorol.*, *5*, 243–262.

Crow, W. T. (2003), Correcting land surface model predictions for the impact of temporally sparse rainfall rate measurements using an ensemble Kalman filter and surface brightness temperature observations (2003), *J. Hydrometeorol.*, *4*, 960–973.

Crow, W. T., and M. J. van den Berg (2010), An improved approach for estimating observation and model error parameters for soil moisture data assimilation, *Water Resour. Res.*, *46*, W12519, doi:10.1029/2010WR009402.

Crow, W. T., and E. Van Loon (2006), The impact of incorrect model error assumptions on the sequential assimilation of remotely sensed surface soil moisture, *J. Hydrometeorol.*, *8*, 421–431.

Crow, W. T., G. F. Huffman, R. Bindlish, and T. J. Jackson (2009), Improving satellite rainfall accumulation estimates using spaceborne soil moisture retrievals, *J. Hydrometeorol.*, *10*, 199–212.

Drusch, M., E. F. Wood, and H. Gao (2005), Observation operators for the direct assimilation of TRMM microwave imager retrieved soil moisture, *Geophys. Res. Lett.*, *32*, L15403, doi:10.1029/2005GL023623.

Entekhabi, D., et al. (2010), The Soil Moisture Active and Passive (SMAP) Mission, *Proc. IEEE*, *98*(5), 704–716, doi:10.1109/JPROC.2010.2043918.

Gebremichael, M., and F. Hossain (2009), *Satellite Rainfall Applications for Surface Hydrology*, Springer, New York.

Harris, A., S. Rahman, F. Hossain, L. Yarborough, A. C. Bagtzoglou, and G. Easson (2007), Satellite-based flood modeling using TRMM-based rainfall products, *Sensors*, *7*(12), 3416–3427.

Higgins, R. W., W. Shi, and E. Yarosh (2000), Improved United States precipitation quality control system and analysis, *NCEP/Clim. Predict. Cent. Atlas 7*, 40 pp., Clim. Predict. Cent., Camp Springs, Md.

Hossain, F., and E. N. Anagnostou (2006a), A two-dimensional satellite rainfall error model, *IEEE Trans. Geosci. Remote Sens.*, *44*, 1511–1522.

Hossain, F., and E. N. Anagnostou (2006b), Assessment of a multidimensional satellite rainfall error model for ensemble generation of satellite rainfall data, *IEEE Geosci. Remote Sens. Lett.*, *3*(3), 419–423, doi:10.1109/LGRS.2006.873686.

Hossain, F., E. N. Anagnostou, and T. Dinku (2004), Sensitivity analysis of satellite rainfall retrieval and sampling error on flood prediction uncertainty, *IEEE Trans. Geosci. Remote Sens.*, *42*, 130–139, doi:10.1109/TGRS.2003.818341.

Huffman, G. J., R. F. Adler, D. T. Bolvin, G. Gu, E. J. Nelkin, K. P. Bowman, Y. Hong, E. F. Stocker, and D. B. Wolff (2007), The TRMM multisatellite precipitation analysis: Quasi-global, multi-year, combined-sensor precipitation estimates at fine scale, *J. Hydrometeorol.*, *8*, 28–55.

Huffman, G. J., R. F. Adler, D. T. Bolvin, and E. J. Nelkin (2010), The TRMM Multi-satellite Precipitation Analysis (TMPA), in *Satellite Rainfall Applications for Surface Hydrology*, edited by F. Hossain and M. Gebremichael, pp. 3–22, Springer, Dordrecht, Netherlands.

Jackson, T. J., M. Cosh, R. Bindlish, P. Starks, D. Bosch, M. Seyfried, D. Goodrich, S. Moran, and D. Du (2010), Validation of Advanced Microwave Scanning Radiometer soil moisture products, *IEEE Trans. Geosci. Remote Sens.*, *48*(12), pp. 4256–4272, doi:10.1109/TGRS.2010.2051035.

Janowiak, J. P. Xie, R. J. Joyce, M. Chen, and Y. Yarosh (2004), Validation of satellite-derived rainfall estimates and numerical model forecasts of precipitation over the United States, paper presented at the 2nd International Precipitation Working Group Meeting, World Meteorological Organization, Monterey, Calif., 25–28 Oct.

Kerr, Y. H., P. Waldteufel, J.-P. Wigneron, J.-M. Martinuzzi, J. Font, and M. Berger (2001), Soil moisture retrieval from space: The Soil Moisture and Ocean Salinity Mission (SMOS), *IEEE Trans. Geosci. Remote Sens.*, *39*, 1729–1735.

Kummerow, C. (1998), Beamfilling errors in passive microwave rainfall retrievals, *J. Appl. Meteorol.*, *37*, 356–370.

Lebel, T., et al. (2009), AMMA-CATCH studies in the Sahelian region of West Africa: An overview, *J. Hydrol.*, *375*(1–2), 3–13.

Li, L., Y. Hong, J. Wang, R. F. Adler, F. Policelli, S. Habib, D. Irwin, T. Korme, and L. Okello (2009), Evaluation of the real-time TRMM-based multi-satellite precipitation analysis for an operational flood prediction system in Nzoia Basin, Lake Victoria, Africa, *Nat. Hazards*, *50*(1), 109–123, doi:10.1007/s11069-008-9324-5.

Liu, J., and R. Chen (1998), Sequential Monte Carlo methods for dynamic systems, *J. Am. Stat. Assoc.*, *93*(443), 1032–1044.

Mason, I. B. (2003), Binary events, in *Forecast Verification: A Practitioner's Guide in Atmospheric Science*, edited by I. T. Jolliffe and D. B. Stephenson, pp. 37–76, John Wiley, Chichester, U. K.

McCabe, M. F., E. F. Wood, R. Wojcik, M. Pan, J. Sheffield, H. Gao, and H. Su (2008), Hydrological consistency using multi-sensor remote sensing data for water and energy cycle studies, *Remote Sens. Environ.*, *112*(2), 430–444.

Morland, J. C., D. F. Grimes, and T. J. Hewison (2001), Satellite observations of the microwave emissivity of a semi-arid land surface, *Remote Sens. Environ.*, *77*(2), 149–164.

Mougin, E., et al. (2009), The AMMA-CATCH Gourma observatory site in Mali: Relating climatic variations to changes in vegetation, surface hydrology, fluxes and natural resources, *J. Hydrol.*, *375*(1–2), 14–33.

Naeimi, V., K. Scipal, Z. Bartalis, S. Hasenauer, and W. Wagner (2009), An improved soil moisture retrieval algorithm for ERS and METOP scatterometer observations, *IEEE Trans. Geosci. Remote Sens.*, *47*, 1999–2013.

Nagarajan, K., J. Judge, W. D. Graham, and A. Monsivais-Huertero (2011), Particle filter-based assimilation algorithms for improved estimation of root-zone soil moisture under dynamic vegetation conditions, *Adv. Water Resour.*, *34*(4), 433–447, doi:10.1016/j.advwatres.2010.09.019.

Nijssen, B., and D. P. Lettenmaier (2004), Effect of precipitation sampling error on simulated hydrological fluxes and states: Anticipating the global measurement satellites, *J. Geophys. Res.*, *109*, D02103, doi:10.1029/2003JD003497.

Njoku, E. G., T. J. Jackson, V. Lakshmi, T. Chan, and S. V. Nghiem (2003), Soil moisture retrieval from AMSR-E, *IEEE Trans. Geosci. Remote Sens.*, *41*, 215–229.

Pan, M., and E. F. Wood (2007), Data assimilation for estimating the terrestrial water budget using a constrained ensemble Kalman filter, *J. Hydrometeorol.*, *7*, 534–547.

Pan, M., H. Li, and E. Wood (2010), Assessing the skill of satellite-based precipitation estimates in hydrologic applications, *Water Resour. Res.*, *46*, W09535, doi:10.1029/2009WR008290.

Pellarin, T., A. Ali, F. Chopin, I. Jobard, and J.-C. Bergs (2008), Using spaceborne surface soil moisture to constrain satellite precipitation estimates over West Africa, *Geophys. Res. Lett.*, *35*, L02813, doi:10.1029/2007GL032243.

Pellarin, T., T. Tran, J.-M. Cohard, S. Galle, J.-P. Laurent, P. de Rosnay, and T. Vischel (2009), Soil moisture mapping over West Africa with a 30-min temporal resolution using AMSR-E observations and a satellite-based rainfall product, *Hydrol. Earth Syst. Sci.*, *13*, 1887–1896.

Reichle, R. H., and R. D. Koster (2005), Global assimilation of satellite surface soil moisture retrievals into the NASA Catchment land surface model, *Geophys. Res. Lett.*, *32*, L02404, doi:10.1029/2004GL021700.

Reichle, R. H., D. B. McLaughlin, and D. Entekhabi (2002), Hydrologic data assimilation with the ensemble Kalman filter, *Mon. Weather Rev.*, *130*, 103–114.

Scipal, K., T. Holmes, R. de Jeu, V. Naeimi, and W. Wagner (2008), A possible solution for the problem of estimating the error structure of global soil moisture data sets, *Geophys. Res. Lett.*, *35*, L24403, doi:10.1029/2008GL035599.

Steiner, M., T. L. Bell, Y. Zhang, and E. F. Wood (2003), Comparison of two methods for estimating the sampling-related uncertainty of satellite rainfall averages based on a large radar dataset, *J. Clim.*, *16*, 3759–3778.

Tobin, K. J., and M. E. Bennett (2010), Adjusting satellite precipitation data to facilitate near real-time hydrologic modeling, *J. Hydrometerol.*, *11*, 967–979.

Wojcik, R., D. McLaughin, A. G. Konings, and D. Entekhabi (2009), Conditioning stochastic rainfall replicates on remote sensing data, *IEEE Trans. Geosci. Remote Sens.*, *47*, 2436–2449.

W. T. Crow, Hydrology and Remote Sensing Laboratory, Agricultural Research Service, USDA, 10300 Baltimore Ave., Rm. 104, Bldg. 007, BARC-W, Beltsville, MD 20705, USA. (wade.crow@ars.usda.gov)

G. J. Huffman, SSAI/NASA Goddard Space Flight Center, Code 613.1, Greenbelt, MD 20771, USA.

T. Pellarin, Laboratoire d'Étude des Transferts en Hydrologie et Environnement, Bâtiment CERMO, Domaine universitaire, BP 53, F-38041 Grenoble CEDEX 9, France.

M. J. van den Berg, Laboratory of Hydrology and Water Management, Ghent University, Coupure Links 653, B-9000 Ghent, Belgium.